Response of electrically coupled spiking neurons: A cellular automaton approach

Lucas S. Furtado* and Mauro Copelli†

Laboratório de Física Teórica e Computacional, Departamento de Física, Universidade Federal de Pernambuco, 50670-901 Recife, PE, Brazil

(Received 22 December 2004; revised manuscript received 6 September 2005; published 12 January 2006)

Experimental data suggest that some classes of spiking neurons in the first layers of sensory systems are electrically coupled via gap junctions or ephaptic interactions. When the electrical coupling is removed, the response function (firing rate vs. stimulus intensity) of the uncoupled neurons typically shows a decrease in dynamic range and sensitivity. In order to assess the effect of electrical coupling in the sensory periphery, we calculate the response to a Poisson stimulus of a chain of excitable neurons modeled by n-state Greenberg-Hastings cellular automata in two approximation levels. The single-site mean field approximation is shown to give poor results, failing to predict the absorbing state of the lattice, while the results for the pair approximation are in good agreement with computer simulations in the whole stimulus range. In particular, the dynamic range is substantially enlarged due to the propagation of excitable waves, which suggests a functional role for lateral electrical coupling. For probabilistic spike propagation the Hill exponent of the response function is $\alpha=1$, while for deterministic spike propagation we obtain $\alpha=\frac{1}{2}$, which is close to the experimental values of the psychophysical Stevens exponents for odor and light intensities. Our calculations are in qualitative agreement with experimental response functions of ganglion cells in the mammalian retina.

DOI: 10.1103/PhysRevE.73.011907 PACS number(s): 87.19.La, 87.10.+e, 87.18.Sn, 05.45.−a

I. INTRODUCTION

Unveiling how neuronal activity represents and processes sensory information remains a very difficult problem, despite theoretical and experimental efforts undertaken by neuroscientists for the last several decades (for a recent review, see [1]). In this broad context, relatively little attention has been devoted to the question of how organisms cope with the several orders of magnitude spanned by the intensities of sensory stimuli [2]. This astonishing ability is most easily revealed in humans by classical results in psychophysics [3]: the perception of the intensity of a given stimulus is experimentally shown to depend on the stimulus intensity r as $\sim\log(r)$ (Weber-Fechner law) or $\sim r^{\alpha}$ (Stevens law), where the Stevens exponent α is typically <1. Those laws have in common the fact that they are *response functions with broad dynamic range*, i.e., they map several decades of stimuli into a single decade of response.

One would like to understand how this broad dynamic range is physically achieved by neuron assemblies. Recent experimental evidence suggests that electrical coupling among neurons in the early layers of sensory systems plays an essential role in weak stimulus detection. Deans *et al.* [4] showed that electrical coupling is present in the mammalian retina via gap junctions (ionic channels that connect neighboring cells). In particular, the spiking response of ganglion cells to light stimulus changes dramatically when the gap junctions are genetically knocked out: both sensitivity and dynamic range are reduced [4].

Another example comes from the olfactory system. The spiking response of isolated olfactory sensory neurons (OSNs) to varying odorant concentration usually presents a narrow dynamic range [5,6]. This is in contrast with the response observed in the next layers of the olfactory bulb: both the glomerular [7,8] and mitral cell [9] responses present a broader dynamic range than the OSNs. In this case, the tightly packed unmyelinated axons of OSNs in the olfactory nerve are believed to interact electrically via ephaptic interactions [10] (i.e., mediated by current flow through the extracellular space), as shown by Bokil *et al.* [11]. In particular, their results indicate that a spike in a single axon can evoke spikes in all other axons of the bundle, suggesting that some computation is performed prior to the glomerular layer.

Motivated by these results, previous papers have shown through numerical simulations that electrical coupling among neurons indeed changes the response function in a way that is consistent with experimental results. Due to the coupling, stimuli generate excitable waves which propagate through the neuron population. The interplay between wave creation and wave annihilation leads to a nonlinear amplification of the spiking response, increasing the sensitivity at low input levels *and* enhancing the dynamic range [12,13]. In one dimension, the robustness of the mechanism is attested by the diversity of models employed: either the biophysically realistic Hodgkin-Huxley equations [12,14], a lattice of nonlinear coupled maps [13,15,16], or the Greenberg-Hastings cellular automata (GHCA) [12,13] yield qualitatively similar results. The same phenomenon has recently been observed in simulations with the two-dimensional GHCA [17].

In this paper we calculate the response of excitable GHCA model neurons [18], where the bidirectional (electrical) coupling is modeled by a probability p of spike transmission. While the uncoupled case $p=0$ can be exactly solved, the coupled case $p>0$ is handled within two mean field approximations, namely at the single-site and pair lev-

*Electronic address: lucas@lftc.ufpe.br

†Corresponding author. Electronic address: mcopelli@df.ufpe.br

els. The aim is to shed light on the analytical behavior of the response function for the one-dimensional case, therefore building on previous efforts which have relied entirely on numerical simulations.

Our focus on the *response* of a *continuously driven* spatially extended excitable system should be carefully confronted with other recent studies, where the main interest has been on phase transitions between an excitable and a self-sustained collective state. For instance, the SIRS model of epidemics in hypercubic lattices has been recently investigated under the mean field and pair approximations [19]. In those contagion models, stationary self-sustained activity becomes stable for sufficiently strong connection among neighbors, a behavior which has been shown to be universal under very general assumptions [20]. Similar results have been obtained for a variety of neuronal models, including collective responses to a localized transient stimulus [21,22], as well as the emergence of sustained activity in complex networks [22,23].

While interesting in its own, the framework of stable-unstable collective transitions does not seem particularly suited for our modeling purposes. To account for sensory responses, the employed GHCA model is an excitable system which always returns to its absorbing state in the absence of stimulus; there are no phase transitions. The refractory period of the GHCA model neurons is absolute (unlike, say, reaction-diffusion lattices), mimicking the deterministic behavior of continuous-time systems like the Hodgkin-Huxley equations or integrate-and-fire models [14]. The only source of stochasticity of the model regards the firing of the neurons. Stimuli can come from spiking neighbors (with probability p) or from an "external" source, which is modeled by a Poisson process and represents sensory input. Therefore, in the limit $p=1$ the dynamics is that of a *deterministic* excitable lattice being *stochastically stimulated*, which casts the problem into the framework of probabilistic cellular automata [24].

The paper is organized as follows. In Sec. II, the GHCA rules are described; Sec. III contains the exact calculations for the response of uncoupled neurons, while in Secs. IV and V results for the coupled case are discussed in the mean field and pair approximations, respectively. Our concluding remarks are presented in Sec. VI.

II. THE MODEL

In the n-state GHCA model [18] for excitable systems, the instantaneous membrane potential of the ith cell ($i=1,\ldots,L$) at discrete time t is represented by $x_i(t) \in \{0,1,\ldots,n-1\}$, $n \geqslant 3$. The state $x_i(t)=0$ denotes a neuron at its resting (polarized) potential, $x_i(t)=1$ represents a spiking (depolarizing) neuron, and $x_i(t)=2,\ldots,n-1$ account for the afterspike refractory period (hyperpolarization). We employ the simplest rules of the automaton: if $x_i(t)=0$, then $x_i(t+1)=1$ only if there is a supra-threshold stimulus at site i; otherwise, $x_i(t+1)=0$. If $x_i(t) \geqslant 1$, then $x_i(t+1)=[x_i(t)+1]$ mod n, regardless of the stimulus. In other words, the rules state that a neuron only spikes if stimulated, after which it undergoes an absolute refractory period before returning to rest.

Whether the neurons are isolated or coupled is implicit in the definition of the supra-threshold stimulus. We assume *external* supra-threshold stimuli to be a Poisson process with rate r (events per second). Hence at each time step an external stimulus arrives with probability

$$\lambda(r) = 1 - e^{-r\tau} \tag{1}$$

per neuron. Notice that $\tau=1$ ms corresponds to the approximate duration of a spike and is the time scale adopted for the time step of the model. The number of states n therefore controls the duration of the refractory period (which corresponds to $n-2$, in ms). In the biological context, r could be related for example with the concentration of a given odorant presented to an olfactory epithelium [5], or the light intensity stimulating a retina [4]. We shall refer to r as the stimulus rate or intensity.

When electrically coupled, neurons at rest can also be stimulated by their neighbors. We define p and q as the probabilities that a resting neuron spikes as a consequence of transmission (ionic current flow) from respectively one or two spiking neighbors [see Eq. (3)]. We keep p and q as two independent parameters in most calculations to show the robustness of some asymptotic results. In the simulations, we concentrate on the more physically intuitive choice of $q=1-(1-p)^2$, where the contributions from two spiking neighbors are independent.

Let $P_t^{(i)}(k)$ be the probability that the ith neuron is in state k at time t. Since the dynamics of the refractory state is deterministic, the equations for $k \geqslant 2$ are simply

$$P_{t+1}^{(i)}(2) = P_t^{(i)}(1)$$

$$P_{t+1}^{(i)}(3) = P_t^{(i)}(2)$$

$$\vdots$$

$$P_{t+1}^{(i)}(n-1) = P_t^{(i)}(n-2). \tag{2}$$

To describe the coupling among first neighbors, let $P_t^{(i)}(k,l,m)$ be the joint probability that sites $i-1$, i and $i+1$ are respectively in the states k, l and m at time t. Following the definitions of λ, p, and q above, the equation for $P_t^{(i)}(1)$ thus becomes

$$\begin{aligned} P_{t+1}^{(i)}(1) = {} & [1-(1-\lambda)(1-q)]P_t^{(i)}(1,0,1) + [1-(1-\lambda)(1-p)] \\ & \times \left(\sum_{k\neq 1}^{n-1} P_t^{(i)}(1,0,k) + \sum_{k\neq 1}^{n-1} P_t^{(i)}(k,0,1) \right) \\ & + \lambda \sum_{k\neq 1}^{n-1} \sum_{l\neq 1}^{n-1} P_t^{(i)}(k,0,l). \end{aligned} \tag{3}$$

Finally, the dynamics for $P_t^{(i)}(0)$ can be obtained by the normalization condition

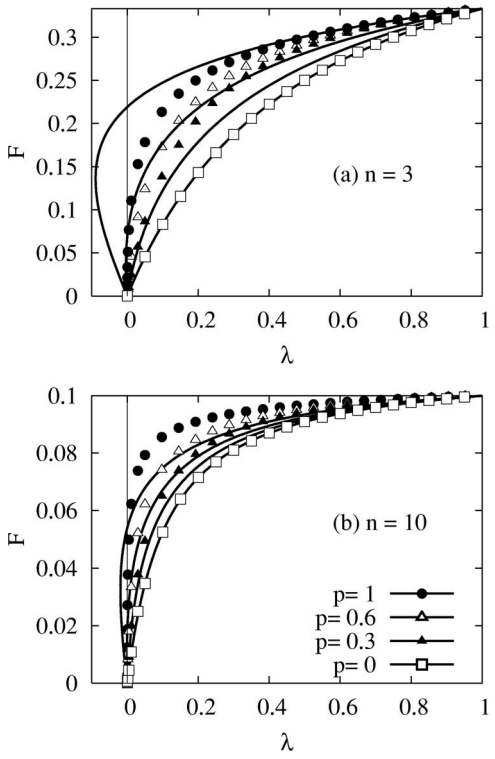

FIG. 1. Response curves for (a) $n=3$ and (b) $n=10$ automata: simulations (symbols) and mean field approximation [lines, according to Eq. (11)]. From bottom to top, $p=0$, 0.3, 0.6, and 1, $q=1-(1-p)^2$. In the simulations, standard deviations over ten runs are smaller than symbol sizes, so error bars are omitted in all figures. Notice the negative slope and multi-valuedness of the single-site approximation for $p>\frac{1}{2}$ and $\lambda\leqslant 0$.

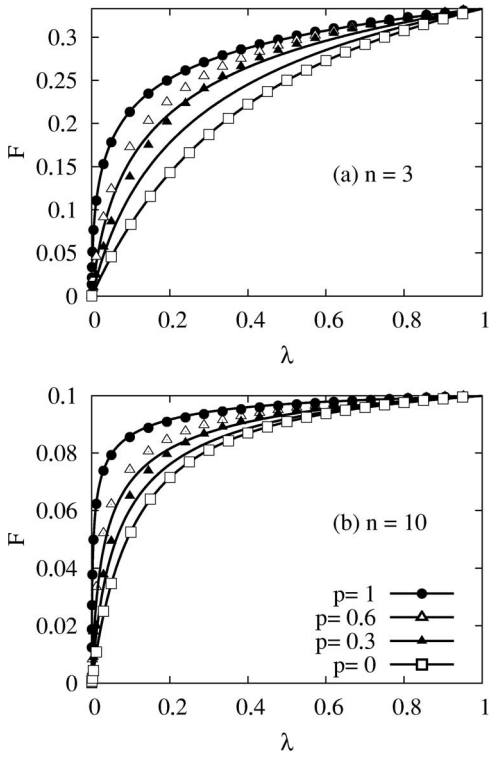

FIG. 2. Response curves for (a) $n=3$ and (b) $n=10$ automata: simulations (symbols) and pair approximation [lines, according to Eqs. (17) and (18)]. From bottom to top, $p=0$, 0.3, 0.6, and 1, $q=1-(1-p)^2$. The pair approximation eliminates the small-λ anomalies of the single-site solution, yielding excellent agreement with simulations for the extreme cases $p=0$ and $p=1$.

$$\sum_{k=0}^{n-1} P_t^{(i)}(k) = 1, \quad \forall\, t,i, \tag{4}$$

which completes the set of equations for one-site probabilities.

It is reasonable to assume homogeneity in the system when $L\to\infty$, so we can drop the superscript (i) in Eqs. (2)–(4) and in what follows. We also expect isotropy (right-left symmetry) in the probabilities: $P_t(k,l)=P_t(l,k)$, $P_t(k,l,m)=P_t(m,l,k)$, etc. Recalling the normalization condition $\Sigma_{j_1=0}^{n-1}P_t(j_1,j_2,\ldots,j_m)=P_t(j_2,\ldots,j_m)$, one can rewrite Eq. (3) as

$$\begin{aligned} P_{t+1}(1) = {} & \lambda P_t(0) + 2p(1-\lambda)P_t(1,0) \\ & + (1-\lambda)(q-2p)P_t(1,0,1). \end{aligned} \tag{5}$$

The stationary value of any joint probability will be denoted by omitting the subscript t, thus $P(\bullet)\equiv\lim_{t\to\infty}P_t(\bullet)$. We start by solving Eqs. (2) and (4) in the stationary state, which together yield

$$P(0) = 1-(n-1)P(1), \tag{6}$$

a result which is exact and holds $\forall p,q$.

We are interested in obtaining the behavior of $P(1)$ as a function of λ (or r). Note that $P(1)$ coincides with the average firing rate per neuron (measured in spikes per ms, according to the choice of τ) in the limit $L,t\to\infty$. In simulations, firing rates have been calculated by division of the total number of spikes in the chain by LT, where $T\sim\mathcal{O}(10^5)$ and $L\sim\mathcal{O}(10^5)$ were the typical number of time steps and model neurons employed. We define $F(\lambda)\equiv P(1)$ as the response function of the system.

Due to the absolute nature of the refractory period, the maximum firing rate of the model neurons is $F_{max}\equiv 1/n$, a result which is easily obtained $\forall p,q$ by setting $\lambda=1$ in Eqs. (5) and (6). The dynamic range δ_λ of the response curve $F(\lambda)$ follows the definition commonly employed in biology [5,25]:

$$\delta_\lambda = 10\log_{10}\left(\frac{\lambda_{0.9}}{\lambda_{0.1}}\right), \tag{7}$$

where λ_x satisfies

$$F(\lambda_x) = xF_{max}. \tag{8}$$

The dynamic range is therefore the number of decibels of input which are mapped into the $\simeq$9.5 dB of output comprised in the $[0.1F_{max},0.9F_{max}]$ interval (see Fig. 3). In the biological context of the model, it measures the ability of the system to discriminate different orders of magnitude of

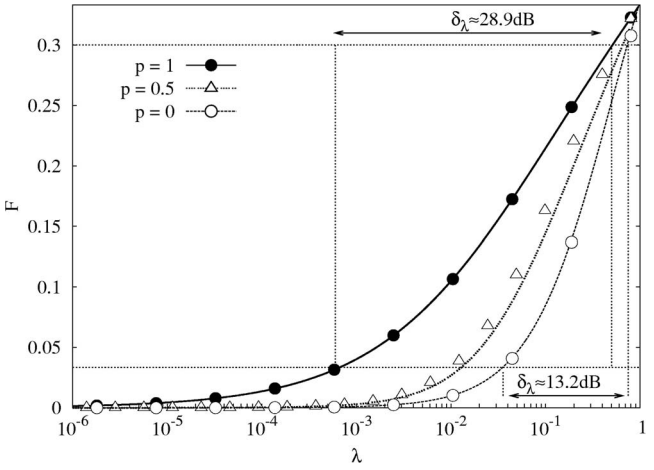

FIG. 3. Linear-log plot of the response curve for $n=3$ automata with $p=q=1$ (filled circles), $p=0.5$ and $q=1-(1-p)^2$ (open triangles), and $p=q=0$ (open circles). Lines correspond to the pair approximation. Horizontal lines are $F=0.1F_{max}$ and $F=0.9F_{max}$, vertical lines are $\lambda=\lambda_{0.1}$ and $\lambda=\lambda_{0.9}$, and arrows illustrate the dynamic range δ_λ [Eq. (7)] for $p=0$ and $p=1$. The dynamic range of a chain of neurons with deterministic spike propagation is about twice as large as that of its uncoupled counterpart.

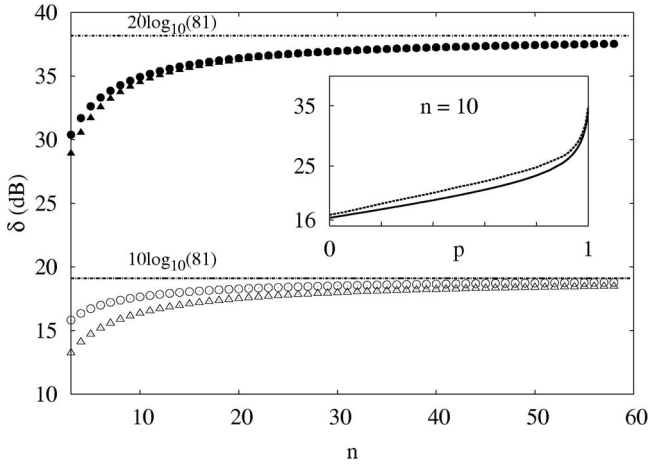

FIG. 4. Dynamic ranges (triangles for δ_λ, circles for δ_r) as a function of the number of states of the GHCA, obtained from the stationary solution of the pair approximation. Open (filled) symbols correspond to the $p=q=0$ ($p=q=1$) case. Inset: δ_λ as a function of p for $n=10$ for simulations (dashed line) and pair approximation (solid line). In spite of the underestimation of the response observed in Fig. 2, the pair approximation is able to reproduce the behavior of the dynamic range as a function of the probability of spike transmission.

stimulus intensity. We will show below that if one chooses to calculate δ_r using $r_x \equiv -\tau^{-1}\ln(1-\lambda_x)$ instead of λ_x in Eq. (7), results are essentially unchanged.

III. UNCOUPLED NEURONS

The uncoupled case $p=q=0$ can be exactly solved by taking the limit $t\to\infty$ in Eq. (5) which, together with Eq. (6), yields

$$P(1) = f(\lambda) = \frac{\lambda}{1+(n-1)\lambda}. \tag{9}$$

This linear saturating response is depicted for $n=3$ (Figs. 1–3) and $n=10$ (Figs. 1 and 2), in complete agreement with simulations. It belongs to the family of Hill functions defined by $H_\alpha(x) \equiv Cx^\alpha/(x_0^\alpha + x^\alpha)$, where the Hill exponent in this case is $\alpha=1$.

The dynamic range can be promptly calculated: $\delta_\lambda(n) = 10\log_{10}[(1+9n)/(1+n/9)]$ and $\delta_r(n) = 10\log_{10}\{\ln(1+9/n)/\ln[1+1/(9n)]\}$, both of which rapidly converge to $10\log_{10}(81) \simeq 19$ dB for moderate values of n (see lower curves in Fig. 4). As we shall see, the electrical coupling can lead to dynamic ranges typically twice as large.

IV. COUPLED NEURONS: MEAN FIELD APPROXIMATION

As can be seen in Eq. (5), $P_t(1)$ depends on two- and three-site probabilities, and in general k-site probabilities depend on up to $(k+2)$-site probabilities. The dynamical description of the system thus requires an infinite hierarchy of equations. The mean field approximation at the single-site level corresponds to the simplest truncation of this hierarchy and consists in discarding the influence of all neighbors in the conditional probabilities [26], thus $P_t(j_1|j_2,\ldots,j_m) \approx P_t(j_1)$, which leads to

$$P_t(j_1,\ldots,j_m) \approx \prod_{k=1}^{m} P_t(j_k). \tag{10}$$

In this approximation, Eq. (5) becomes

$$P_{t+1}(1) \approx P_t(0)[\lambda + 2p(1-\lambda)P_t(1) + (q-2p)(1-\lambda)P_t(1)^2], \tag{11}$$

which, together with Eq. (6), can be used to eliminate $P(0)$ and render $P(1)=F(\lambda)$ implicitly through the relation

$$\lambda \approx \frac{(1-2p)F + (2pn-q)F^2 + (n-1)(q-2p)F^3}{[1-(n-1)F][1-2pF+(2p-q)F^2]}. \tag{12}$$

As a consistency check, notice that setting $p=q=0$ in Eq. (12) recovers Eq. (9) (in other words, mean field is exact for the uncoupled case, as it should). However, for $0<p,q\leqslant 1$, $F(\lambda)$ as given by Eq. (12) yields in general a poor agreement with numerical simulations, as can be seen in Fig. 1 for different values of p. When $\lambda \simeq 0$, Eq. (12) predicts $F \simeq \lambda/(1-2p)$, which leads to obviously nonphysical results for $p \geqslant \frac{1}{2}$ (see leftmost part of Fig. 1). In particular, $F(\lambda)$ is multi-valued, leading to $\lim_{\lambda\to 0^+} F \neq 0$. The mean field result therefore suggests a transition to an ordered state at $\lambda=0$ which is simply forbidden by the automaton rules [27]. By generalizing Eq. (11), this failure to predict the absorbing state of the system can in fact be extended to regular lattices with coordination z, where the single-site approximation yields $F \underset{\lambda\to 0}{\simeq} \lambda/(1-pz)$. Since this level of approximation is

clearly not satisfactory for the calculation of the dynamic range, a refinement is needed.

V. COUPLED NEURONS: PAIR APPROXIMATION

The pair approximation consists in keeping the influence of only one neighbor in the conditional probabilities [26], thus $P_t(j_1|j_2,\ldots,j_m)\approx P_t(j_1|j_2)$. In this case m-site probabilities are reduced to combinations of up to two-site probabilities. In particular, three- and four-site probabilities become [26]

$$P(k,l,m) \approx \frac{P(k,l)P(l,m)}{P(l)}, \tag{13a}$$

$$P(j,k,l,m) \approx \frac{P(j,k)P(k,l)P(l,m)}{P(k)P(l)}. \tag{13b}$$

It is therefore possible to rewrite Eq. (5) in this approximation:

$$P_{t+1}(1) \approx \lambda P_t(0) + (1-\lambda)P_t(1,0) \times\left(2p + (q-2p)\frac{P_t(1,0)}{P_t(0)}\right). \tag{14}$$

Equation (14), on its turn, depends on $P_t(1,0)$, whose evolution can be exactly obtained (up to homogeneity and isotropy assumptions):

$$\begin{aligned} P_{t+1}(1,0) = {} & \lambda P_t(n-1,0) + p(1-\lambda)P_t(n-1,0,1) \\ & + \lambda(1-\lambda)P_t(0,0) + p(1-\lambda)(1-2\lambda)P_t(1,0,0) \\ & - p^2(1-\lambda)^2 P_t(1,0,0,1). \end{aligned} \tag{15}$$

With the help of the pair approximation in Eqs. (13), Eq. (15) becomes

$$\begin{aligned} P_{t+1}(1,0) \approx {} & P_t(n-1,0)\left(\lambda + p(1-\lambda)\frac{P_t(1,0)}{P_t(0)}\right) \\ & + (1-\lambda)P_t(0,0)\left(\lambda + p(1-2\lambda)\frac{P_t(1,0)}{P_t(0)}\right. \\ & \left. - p^2(1-\lambda)\frac{P_t(1,0)^2}{P_t(0)^2}\right). \end{aligned} \tag{16}$$

Since $P_t(j,0)$ depends on $P_t(j-1,0)$ and $P_t(j-1,n-1)$, and $P_t(0,0)$ depends, among others, on $P_t(n-1,n-1)$, all the equations for two-site probabilities are in principle required for the dynamical description of the system. Together with the equations for single-site probabilities, they form a $(n^2+3n)/2$-dimensional map whose stationary stable solution can be analytically studied. While the Appendix contains details of the derivation of those equations, we discuss the main results below.

The main point to be noted is that the calculation of the stationary state presents additional difficulties when $n\geqslant 4$. In that case, the pair probabilities $P(j,0)$ with $2\leqslant j\leqslant n-2$ have the same stationary value, but differ from $P(n-1,0)$. In particular, for $p=q=1$ one obtains $P(j,0)=0$ [$2\leqslant j\leqslant n-2$, see Eq. (A10)], which in turn leads to many other vanishing probabilities and gives the deterministic case a sparse stationary matrix [see Eqs. (A4), (A5), and (A8)]. Those terms do not exist for the $n=3$ case, which makes its analysis considerably simpler. In either case, for $n\geqslant 3$ one obtains the reasonable result $P(n-1,0)\approx P(1,0)$, the l.h.s. (r.h.s.) being associated to the end (beginning) of an excitable wave front [see Eq. (A12)]. Combining these results, a normalization condition and the linearity of Eq. (16) in $P_t(0,0)$, we obtain (see the Appendix)

$$\begin{aligned} & P(0) - P(1,0)\left[2 + (n-3)\left(\frac{(1-p)P(0) + (p-q)P(1,0)}{P(0) - pP(1,0)}\right)\right] \\ & \approx \frac{P(1,0)P(0)[P(0) - pP(1,0)]}{\lambda P(0)^2 + p(1-2\lambda)P(0)P(1,0) - p^2(1-\lambda)P(1,0)^2}, \end{aligned} \tag{17}$$

which is valid $\forall n\geqslant 3$. Consider now the stationary state of Eqs. (6) and (14). They can be combined in a quadratic equation for $P(1,0)$, yielding

$$(2p-q)P(1,0) \approx G_{\pm}[P(0)] \equiv pP(0) \pm \sqrt{\frac{P(0)\{P(0)[(n-1)p^2 + 2p - q + \lambda(n-1)(2p-p^2-q)] + (q-2p)\}}{(n-1)(1-\lambda)}}. \tag{18}$$

Since $P(1,0)$ must vanish $\forall p,q$ in the limit $\lambda\to 0$, G_- is the only acceptable solution.

The solution of Eqs. (17) and (18) determines $P(0)$ as a function of λ. Instead of numerically solving them, we iterate the $(n^2+3n)/2$-dimensional map involving the one- and two-site probabilities for each value of λ until it converges to its stationary state. Despite the growing number of equations with n, this method has the advantage of avoiding unstable fixed points [26] [Eqs. (17) and (18) can have more than one solution]. Once $P(0)$ is known, the response $P(1)=F(\lambda)$ is obtained via Eq. (6).

A. Deterministic spike propagation ($p=1$)

Ordinary differential equations (ODEs) are the standard modeling tool in computational neuroscience. This is due to the fact that, despite the stochastic nature of the opening and closing of individual ionic channels, a neuron containing a large number of such channels can very often be extremely well described by a deterministic dynamics [14] (an approach which has been established since the seminal work of Hodgkin and Huxley [28]). In the present context, it is therefore important to address the case $p=1$. This limit is consistent with a variety of scenarios in which, in addition to the dynamics of individual neurons, spike transmission is also well described by deterministic behavior. Specifically regarding our present study, deterministic spike transmission due to electrical coupling has previously been employed in the literature to model axo-axonal interactions both via ephaptic interactions (e.g., in the olfactory nerve [11]) and gap junctions (e.g., in the hippocampus [27,29]). This is in contrast with, say, dendro-dendritic gap junctions or chemical synapses (in the latter case, synaptic transmission can sometimes be as low as 10% due to the inherent stochasticity in the process of neurotransmitter release [14,30]), where the $p=1$ limit can hardly be expected to apply. As we shall see in the following, in addition to its biological relevance, the response function for $p=1$ also has a different characteristic exponent which will help us understand the limiting behavior for $p \lesssim 1$.

Figure 2 shows the excellent agreement between the pair approximation and the simulations when $p=q=1$. One observes that the response is particularly enhanced in the low stimulus range. This feature is best seen in the logarithmic scale of Fig. 3: in comparison with the uncoupled case $p=0$, the effect of the electrical interaction is to increase the sensitivity of the response for more than a decade, leading to a dramatic rise of the dynamic range.

For each value of n, we can thus obtain the stationary response $F(\lambda)$ and the dynamic ranges δ_λ and δ_r in the pair approximation. Even though the response curve changes considerably for varying n (since F is bounded by $F_{max}=1/n$, see Fig. 2), the dynamic range levels off smoothly, as can be seen in Fig. 4. For increasing n, the dynamic range of the $p=q=1$ case approaches twice the value for the uncoupled case. The fact that this result holds for both δ_r and δ_λ can be understood on the basis of the low-stimulus amplification, which plays the central role in the phenomenon: in this regime λ is approximately linear in r. Should one choose a different relationship $\lambda(r)$, δ_r would obviously have different values, but the drastic enhancement in the response due to the electrical coupling would not be affected.

In order to understand the low-stimulus amplification induced by the coupling, we have analyzed Eqs. (17) and (18) when $\lambda \simeq 0$. Inspection of Fig. 2 and previous numerical simulations [12] suggests that $P(1) \simeq C\lambda^\alpha$, with $\alpha<1$. This ansatz can be inserted into Eqs. (6), (17), and (18) for general p and q, yielding $\alpha=\frac{1}{2}$ *and* $p=1$ as solutions. Deterministic spike propagation therefore leads to a power law response

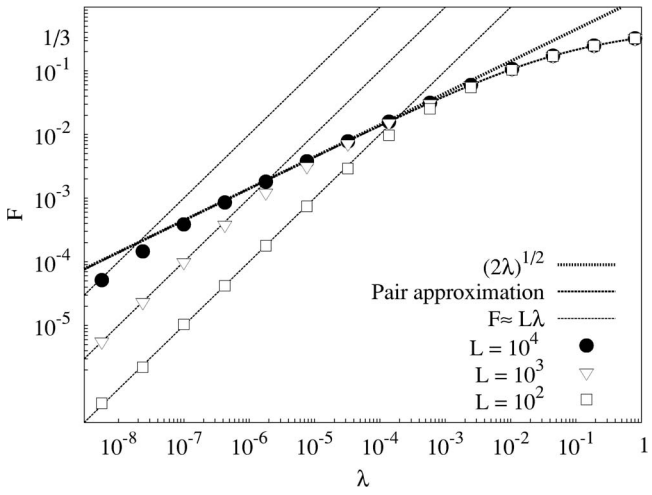

FIG. 5. Log-log plot of the response curve for $p=q=1$. Pair approximation (solid lines) and simulations (symbols) follow a power law $(\alpha=\frac{1}{2})$ for weak stimuli, while finite size effects lead to a linear response $F \simeq L\lambda$ (dotted lines) for $\lambda \lesssim \lambda_c(L)$.

$$F(\lambda) \overset{\lambda \to 0}{\simeq} \sqrt{2\lambda}, \tag{19}$$

a result that holds $\forall n,q$, as should be expected. This power law suggests a Hill function with $\alpha=\frac{1}{2}$, which is an excellent approximation for $F(\lambda)$ in the whole λ interval when n is large. This result explains the doubling of the dynamic range as compared to the uncoupled case and is reminiscent of reaction-diffusion processes modeled by lattice gases [31–34] and partial differential equations [35]. Since the Hill function can be regarded as a saturating Stevens law, it is interesting to note that the experimental values of the Stevens exponents for light and smell intensities are respectively $\alpha \simeq 0.5$ and $\alpha \simeq 0.6$ [3].

Let us now consider a chain with *finite* L and a very small value of λ such that a single external stimulus occurs in a given time interval. In this case, the deterministic nature of the propagation would lead to L spikes in the chain, while a single spike would be observed if the neurons were uncoupled. One would thus have $F \simeq Lf$, and since $f \overset{\lambda \to 0}{\simeq} \lambda$ [from Eq. (9)] we obtain $F \overset{\lambda \to 0}{\simeq} L\lambda$. This corresponds to a linear regime where excitable waves do not interact. If one increases λ, waves will start annihilating each other, leading to the power law response of Eq. (19), as can be clearly seen in Fig. 5. For a given system size L, there is therefore a crossover value $\lambda_c(L) \simeq 2/L^2$ from a linear to a nonlinear response. In an infinite chain, there is no linear response since for any nonzero stimulus rate two excitable waves will inevitably interact.

To assess the finite size effects in the biological context of the model, we notice that the dynamic range will be affected only if $\lambda_c(L) \gtrsim \lambda_{0.1}$, that is, for $L \lesssim 20n$. For neurons with refractory periods of the order of tens of ms, neuronal assemblies with $L \gtrsim 10^{3-4}$ should therefore be well approximated by the limit $L \to \infty$, as can be seen in Fig. 6. It is important to emphasize, however, that even small chains dominated by

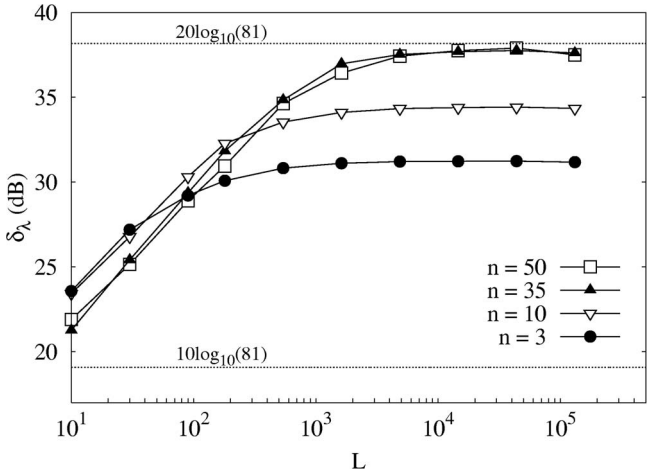

FIG. 6. Dynamic range as a function of the system size L for $p=q=1$. Lines are just guides to the eye.

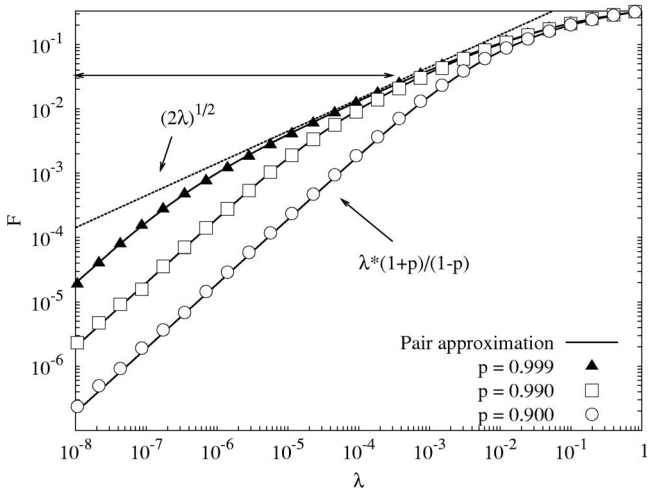

FIG. 7. Log-log plot of the response curve: pair approximation (solid lines) and simulations (symbols) with $q=1-(1-p)^2$ and $n=3$. For $p\lesssim 1$, there is a crossover between $\alpha=1$ and $\alpha=\frac{1}{2}$. The horizontal arrow shows $0.1F_{max}$.

finite size effects still possess dynamic ranges which are significantly larger than those of the uncoupled case. For $\lambda_{0.1}\lesssim\lambda_c(L)$, the dynamic range increases approximately logarithmically with the total number of connected neurons, a result which holds for regular lattices in any dimension [17].

B. Probabilistic spike propagation ($p\neq 1$)

For $p\neq 1$, communication between spiking and resting neurons may eventually fail. This provides us with the simplest test under which the robustness of the mechanism for dynamic range enhancement can be checked. From the biological point of view, this regime could be useful for modeling networks of neurons connected by chemical synapses, for instance.

We start the analysis of the $p\neq 1$ case by noticing in Figs. 2 and 3 that the agreement between simulations and the pair approximation is better than the mean field results (especially in the low-stimulus region), but certainly not as good as in the extreme cases $p=0$ and $p=1$. This inevitably affects the estimation of the dynamic range via the stationary state of the pair approximation (see below), but nonetheless allows us to understand qualitatively how the response changes as p varies.

As pointed out in the preceding section, the dynamic range is enhanced for $p=1$ primarily due to the low-stimulus amplification associated to the propagation of excitable waves. As opposed to the deterministic case, however, for $p\neq 1$ a single excitable wave traveling in an infinite chain initially at rest will eventually die out. We should therefore expect a qualitative change in the response function for $\lambda\simeq 0$. This is indeed confirmed by reinserting the ansatz $P(1)\simeq C\lambda^\alpha$ in Eqs. (6), (17), and (18) without the constraint $\alpha<1$. In this case, the linear behavior suggested by the plots in Fig. 2 is easily confirmed:

$$F(\lambda)\overset{\lambda\to 0}{\simeq}\left(\frac{1+p}{1-p}\right)\lambda, \tag{20}$$

which is again valid $\forall n,q$. Therefore, the low-stimulus response for $p<1$ is governed by $\alpha=1$, which is confirmed by the simulations displayed in Fig. 7. Interestingly, such a change in exponent for $p<1$ seems to be absent from reaction-diffusion models in lattice gases [31–34] as well as partial differential equations [35].

Thanks to the growing coefficient in Eq. (20), for $p\lesssim 1$ the proximity to the transition that occurs at $p=1$ produces a crossover in the response from a linear to a square root behavior, dismissing the suspicion that a larger exponent might severely deteriorate the enhancement of the dynamic range (see Fig. 7). In particular, notice that, for $p\lesssim 1$, $\alpha=\frac{1}{2}$ is the dominant exponent at $F=0.1F_{max}$, which is used to calculate the dynamic range (see horizontal arrow in Fig. 7). This explains the smooth monotonic increase in δ_λ with p, as shown in the inset of Fig. 4, even though the exponent changes discontinuously at $p=1$. On the one hand, we observe that deterministic spike propagation ($p=1$) is certainly not essential for the enhancement of the dynamic range, in the sense that any $p>0$ yields a better response than uncoupled neurons. On the other hand, it is interesting to point out that, as p is varied from 0 to 1, the increase in dynamic range is particularly pronounced for $p\gtrsim 0.9$. This is in agreement with the conjecture that the reliability of electrical coupling among spiking neurons could indeed play a significant role in early sensory processing.

VI. CONCLUDING REMARKS

We have calculated the collective response to a Poisson stimulus of a chain of electrically coupled excitable neurons modeled by n-state Greenberg-Hastings cellular automata. The single-site mean field approximation has been shown to give poor results, failing to predict the absorbing state of the lattice in the absence of stimulus for $p\geqslant\frac{1}{2}$. The pair approximation yields a response curve which agrees reasonably well with simulations *in the whole stimulus range*. It is interesting to remark that the agreement is particularly good when $p=q=1$, a deterministic regime in which the GHCA lattice

mimics a system of coupled nonlinear ODEs. This reinforces an interesting perspective in the context of computational neuroscience: the possibility of applying techniques from nonequilibrium statistical mechanics to the study of spatially extended nonlinear systems.

The enhancement of the dynamic range in the presence of electrical coupling is due to low-stimulus amplification. For uncoupled neurons ($p=0$) the response is governed by the Hill exponent $\alpha=1$, leading to a dynamic range of ~ 19 dB. For coupled neurons this value can be doubled in the limit $p=q\to 1$, when the Hill exponent becomes $\alpha=\frac{1}{2}$. This value is close to Stevens exponents observed in psychophysical experiments of smell and light intensities. For $0<p<1$, the exponent remains $\alpha=1$, but the dynamic range increases smoothly, which can be understood on the basis of the crossover behavior observed in the response function for $p\lesssim 1$.

In the context of experiments at the cellular level, the enhancement of the dynamic range associated to an increase in sensitivity is also observed in both the olfactory [8] and visual [4] systems. While the dynamic range of OSNs (the neurons which perform the initial transduction) is about ~ 10 dB [5,6], the glomeruli (the next processing layer) have dynamic ranges at least twice as large [8]. It remains to be investigated experimentally whether this enhancement is indeed due to ephaptic interactions among the unmyelinated OSN axons in the olfactory nerve.

Stronger experimental support for our conjecture on the role of electrical interactions is available for the mammalian retina. Deans *et al.* [4] have measured the firing rates of on-center ganglion cells for varying light intensity (measured in isomerized molecules of rhodopsin per rod per second, or $\mathrm{Rh}^*/\mathrm{rod/s}$). The response curves have been obtained for both wild type (WT) mice as well as mice in which the expression of the protein connexin36 (responsible for the gap junction intercellular channels) has been genetically knocked out (Cx36-KO). The difference in the response curves can be seen in Fig. 8. They present the same qualitative behavior of the curves shown in Fig. 3, exhibiting an increase in dynamic range in the presence of electrical coupling: 14 dB for Cx36-KO and 23 dB for WT, values which are of the same order as those of Fig. 6. In particular, the exponent of the "coupled" (WT) case is $\alpha\simeq 0.58$ (see inset), which is slightly larger than what is obtained in the pair approximation.

The quantitative agreement between the analytical and experimental curves is limited. On the one hand, the theoretical $n=3$ curve can provide a good fit of the Cx36-KO data for $p=q=0$, while the coupled case $p=q=1$ does not adjust well to the WT data. For $n=10$ and $p=q=1$, on the other hand, the WT data are well matched by simulations with a finite $L=20$ system (staying below the $L\to\infty$ pair approximation), but for $p=q=0$ the same $n=10$ automata are unable to give a good fit of the Cx36-KO data. The difficulties of a quantitative match are not surprising: the retina is organized in layers which have, to first order, a two-dimensional structure; signal processing from the photoreceptors to the ganglion cells involves a complex intermediate neuronal circuit (with bipolar, horizontal and amacrine cells [36]); and individual neurons themselves can have subtle dynamical properties (such as adaptation, for instance). All these properties are clearly absent from our simple one-dimensional CA model. Yet it correctly predicts the reduction in the dynamic range of a neuronal system which loses electrical coupling among its cells.

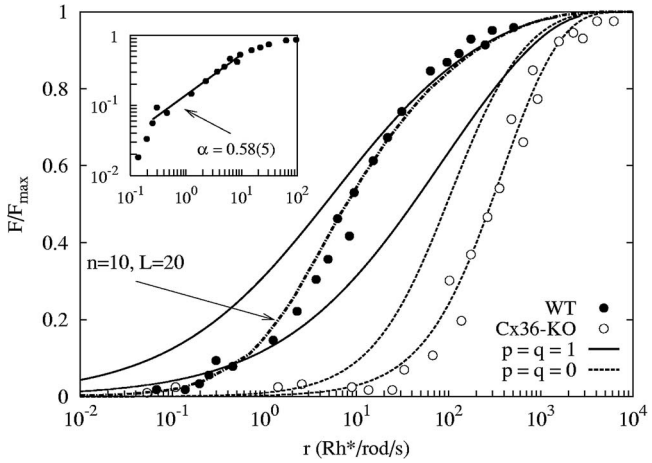

FIG. 8. Experimental response curves (normalized firing rate vs. light intensity) of retinal on-center ganglion cells in linear-log (main plot) and log-log (inset) scales (data extracted from Fig. 6 of Ref. [4]). Filled (open) circles are for WT (Cx36-KO) mice, solid (dashed) lines show the results of the pair approximation, thus $L\to\infty$, with $p=q=1$ ($p=q=0$). Upper curves are for $n=10$, lower curves are for $n=3$. The dot-dashed line corresponds to simulations with $n=10$, $p=q=1$, and $L=20$.

In order to have a quantitative agreement between experimental and theoretical curves, additional modeling efforts are needed which incorporate specific details of the system under consideration. However, the response of simple models of excitable media remains an important subject to be studied, precisely because they have the potential to reveal simple mechanisms and scaling relations [35] whose robustness can thereafter be subjected to further testing in experiments and more detailed models. In this context, the simple Greenberg-Hastings CA strikes an interesting balance, on the one hand capturing essential features of collective neuronal dynamics, while on the other hand lending itself to analytical techniques borrowed from nonequilibrium statistical mechanics.

ACKNOWLEDGMENTS

The authors would like to thank O. Kinouchi, S. G. Coutinho, A. C. Roque, R. F. Oliveira, R. Publio, M. J. de Oliveira, and an anonymous referee for useful discussions and comments. LSF is supported by UFPE/CNPq/PIBIC. MC acknowledges support from Projeto Enxoval (UFPE), FACEPE, CNPq, and special program PRONEX.

APPENDIX: THE EQUATIONS FOR TWO-SITE PROBABILITIES

1. Dynamics

In all derivations below, homogeneity and isotropy are assumed. The sign "≈" denotes that the equality holds in the pair approximation [Eqs. (13)]. We start by writing down the equation for $P_t(0,0)$, which holds $\forall n \geqslant 3$:

$$\begin{aligned} P_{t+1}(0,0) &= P_t(n-1,n-1) + 2(1-\lambda)[P_t(n-1,0) \\ &\quad - pP_t(1,0,n-1)] + (1-\lambda)^2[P_t(0,0) \\ &\quad - 2pP_t(1,0,0) + p^2P_t(1,0,0,1)] \\ &\approx P_t(n-1,n-1) + 2(1-\lambda)P_t(n-1,0) \\ &\quad \times\left(1 - p\frac{P_t(1,0)}{P_t(0)}\right) + (1-\lambda)^2P_t(0,0) \\ &\quad \times\left(1 - 2p\frac{P_t(1,0)}{P_t(0)} + p^2\frac{P_t(1,0)^2}{P_t(0)^2}\right). \end{aligned} \tag{A1}$$

The dynamics for two-site probabilities in the refractory period obey a simple recursive rule due to the deterministic evolution of the automata:

$$P_{t+1}(j,k) = P_t(j-1,k-1), \quad 2 \leqslant j,k \leqslant n-1. \tag{A2}$$

On the one hand, diagonal terms $P_t(j,j)$ with $j \geqslant 2$ recursively depend on $P_t(1,1)$, whose dynamics can be written as follows:

$$\begin{aligned} P_{t+1}(1,1) &= \lambda^2P_t(0,0) + 2p\lambda(1-\lambda)P_t(1,0,0) \\ &\quad + p^2(1-\lambda)^2P_t(1,0,0,1) \\ &\approx P_t(0,0)\left(\lambda^2 + 2p\lambda(1-\lambda)\frac{P_t(1,0)}{P_t(0)}\right. \\ &\quad \left. + p^2(1-\lambda)^2\frac{P_t(1,0)^2}{P_t(0)^2}\right). \end{aligned} \tag{A3}$$

Off-diagonal terms, on the other hand, ultimately depend on $P_t(j,1)$. For $j=2$, the equation is simply

$$\begin{aligned} P_{t+1}(2,1) &= (\lambda + p - p\lambda)P_t(1,0) + (1-\lambda)(q-p)P_t(1,0,1) \\ &\approx P_t(1,0)\left[\lambda + (1-\lambda)\left(p + (q-p)\frac{P_t(1,0)}{P_t(0)}\right)\right], \end{aligned} \tag{A4}$$

while for $j \geqslant 3$ one has

$$\begin{aligned} P_{t+1}(j,1) &= \lambda P_t(j-1,0) + p(1-\lambda)P_t(j-1,0,1) \\ &\approx P_t(j-1,0)\left(\lambda + p(1-\lambda)\frac{P_t(1,0)}{P_t(0)}\right). \end{aligned} \tag{A5}$$

Finally, one needs equations for $P_t(j,0)$, $j \geqslant 2$ [recall Eq. (16) for $P_t(1,0)$]. Like in Eq. (A4), the case $j=2$ must be considered separately:

$$\begin{aligned} P_{t+1}(2,0) &= P_t(1,n-1) + (1-\lambda)(1-p)P_t(1,0) + (1-\lambda)(p-q)P_t(1,0,1) \\ &\approx P_t(1,n-1) + (1-\lambda)P_t(1,0)\left((1-p) + (p-q)\frac{P_t(1,0)}{P_t(0)}\right). \end{aligned} \tag{A6}$$

For $j \geqslant 3$, on the other hand, one immediately obtains

$$\begin{aligned} P_{t+1}(j,0) &= P_t(j-1,n-1) + (1-\lambda)[P_t(j-1,0) \\ &\quad - pP_t(j-1,0,1)] \\ &\approx P_t(j-1,n-1) \\ &\quad + (1-\lambda)P_t(j-1,0)\left(1 - p\frac{P_t(1,0)}{P_t(0)}\right), \end{aligned} \tag{A7}$$

which completes the set of all pair equations. Upon iteration of Eqs. (2), (4), (14), (16), (A1), and (A7), normalization conditions properly imposed in the initial conditions are naturally preserved. To determine the response function $P(1)=F(\lambda)$, we wait until the $(n^2+3n)/2$-dimensional map reaches a stationary state for each value of λ. We describe below how the analysis of the stationary state can be reduced to just two equations [Eqs. (17) and (18)].

2. Stationary state

We start by handling the case $n>4$. In the stationary state, the first term on the r.h.s. of Eq. (A7) becomes, via recursive iterations of Eq. (A2),

$$P(j-1,n-1) = P(1,1+n-j), \quad \forall\, j \geqslant 3. \tag{A8}$$

The above result can on its turn be further developed by means of Eq. (A5) as long as $1+n-j \geqslant 3$, rendering the stationary state of Eq. (A7):

$$\begin{aligned} P(j,0) &\approx P(n-j,0)\left(\lambda + p(1-\lambda)\frac{P(1,0)}{P(0)}\right) \\ &\quad + (1-\lambda)P(j-1,0) \\ &\quad \times\left(1 - p\frac{P(1,0)}{P(0)}\right), \quad 3 \leqslant j \leqslant n-2. \end{aligned} \tag{A9}$$

Notice that we have a nonhomogeneous set of $n-4$ linear equations for $x_j \equiv P(j,0): x_j \approx ax_{n-j} + (1-a)x_{j-1}$, where $a \equiv \lambda + p(1-\lambda)P(1,0)/P(0)$ and $x_2 = P(2,0)$ accounts for the

nonhomogeneity in the equations for x_3 and x_{n-2}. The solution of these equations is simply $x_{n-2} \approx x_{n-1} \approx \cdots \approx x_3 \approx x_2$, as can be checked by inspection. The combination of Eqs. (A6) and (A5) in the stationary state, on the other hand, leads to

$$P(j,0) \approx J[P(1,0),P(0)] \equiv P(1,0)\left(\frac{(1-p)P(0)+(p-q)P(1,0)}{P(0)-pP(1,0)}\right), \quad 2 \leqslant j \leqslant n-2. \tag{A10}$$

One therefore obtains

$$P(n-2,0) \approx P(n-3,0) \approx \cdots \approx P(2,0) \approx J[P(1,0),P(0)]. \tag{A11}$$

Finally, notice that $P(n-1,0)$ can be obtained by combination of Eqs. (A7), (A11), and (A4):

$$P(n-1,0) \approx P(1,0), \tag{A12}$$

which completes the proof for $n>4$. For $n=4$, it suffices to invoke Eqs. (A6) and (A5) to show that $P(2,0) \approx J[P(1,0),P(0)]$. With this result, Eq. (A12) holds for $n \geqslant 4$. Finally, for $n=3$, Eqs. (A6) and (A4) together also lead to Eq. (A12).

Invoking the normalization condition $P_t(0)=\Sigma_{j=0}^{n-1} P_t(j,0)$, one can deduce that, on the one hand,

$$P(0,0) = P(0) - 2P(1,0) - (n-3)J[P(1,0),P(0)]. \tag{A13}$$

On the other hand, in the stationary state Eq. (16) depends linearly on $P(0,0)$, so it can be inverted, yielding [after substitution of Eq. (A12)] $P(0,0)$ as a function of $P(1,0)$ and $P(0)$. Equaling this function to Eq. (A13), $P(0,0)$ is eliminated and one obtains Eq. (17).

[1] G. Kreiman, Phys. Life Rev. **1**, 71 (2004).
[2] T. A. Cleland and C. Linster, Neural Comput. **11**, 1673 (1999).
[3] S. S. Stevens, *Psychophysics: Introduction to its Perceptual, Neural and Social Prospects* (Wiley, New York, 1975).
[4] M. R. Deans, B. Volgyi, D. A. Goodenough, S. A. Bloomfield, and D. L. Paul, Neuron **36**, 703 (2002).
[5] J.-P. Rospars, P. Lánský, P. Duchamp-Viret, and A. Duchamp, BioSystems **58**, 133 (2000).
[6] J.-P. Rospars, P. Lánský, P. Duchamp-Viret, and A. Duchamp, Eur. J. Neurosci. **18**, 1135 (2003).
[7] R. W. Friedrich and S. I. Korsching, Neuron **18**, 737 (1997).
[8] M. Wachowiak and L. B. Cohen, Neuron **32**, 723 (2001).
[9] P. Duchamp-Viret, A. Duchamp, and M. Vigouroux, Chem. Senses **15**, 349 (1990).
[10] G. Lowe, Curr. Opin. Neurobiol. **13**, 476 (2003).
[11] H. Bokil, N. Laaris, K. Blinder, M. Ennis, and A. Keller, J. Neurosci. **21**, RC173 (2001).
[12] M. Copelli, A. C. Roque, R. F. Oliveira, and O. Kinouchi, Phys. Rev. E **65**, 060901(R) (2002).
[13] M. Copelli, R. F. Oliveira, A. C. Roque, and O. Kinouchi, Neurocomputing **65–66**, 691 (2005).
[14] C. Koch, *Biophysics of Computation* (Oxford University Press, New York, 1999).
[15] S. M. Kuva, G. F. Lima, O. Kinouchi, M. H. R. Tragtenberg, and A. C. Roque, Neurocomputing **38–40**, 255 (2001).
[16] M. Copelli, M. H. R. Tragtenberg, and O. Kinouchi, Physica A **342**, 263 (2004).
[17] M. Copelli and O. Kinouchi, Physica A **349**, 431 (2005).
[18] J. M. Greenberg and S. P. Hastings, SIAM J. Appl. Math. **34**, 515 (1978).
[19] J. Joo and J. L. Lebowitz, Phys. Rev. E **70**, 036114 (2004).
[20] P. S. Dodds and D. J. Watts, Phys. Rev. Lett. **92**, 218701 (2004).
[21] H. Hasegawa, Phys. Rev. E **67**, 041903 (2003).
[22] A. Roxin, H. Riecke, and S. A. Solla, Phys. Rev. Lett. **92**, 198101 (2004).
[23] T. I. Netoff, R. Clewley, S. Arno, T. Keck, and J. A. White, J. Neurosci. **24**, 8075 (2004).
[24] G. Ódor, Rev. Mod. Phys. **76**, 663 (2004).
[25] S. Firestein, C. Picco, and A. Menini, J. Physiol. (London) **468**, 1 (1993).
[26] A. P. F. Atman, R. Dickman, and J. G. Moreira, Phys. Rev. E **67**, 016107 (2003).
[27] T. J. Lewis and J. Rinzel, Network Comput. Neural Syst. **11**, 299 (2000).
[28] A. L. Hodgkin and A. F. Huxley, J. Neurophysiol. **117**, 500 (1952).
[29] R. D. Traub, D. Schmitz, J. G. R. Jefferys, and A. Draguhn, Neuroscience **92**, 407 (1999).
[30] E. R. Kandel, J. H. Schwartz, and T. M. Jessell, eds., *Essentials of Neural Science and Behavior* (Appleton & Lange, Norwalk, Connecticut 1995).
[31] R. B. Stinchcombe, M. D. Grynberg, and M. Barma, Phys. Rev. E **47**, 4018 (1993).
[32] M. D. Grynberg, T. J. Newman, and R. B. Stinchcombe, Phys. Rev. E **50**, 957 (1994).
[33] M. J. de Oliveira, Phys. Rev. E **60**, 2563 (1999).
[34] J. R. G. de Mendonça and M. J. de Oliveira, J. Stat. Phys. **92**, 651 (1998).
[35] T. Ohta and T. Yoshimura, Physica D **205**, 189 (2005).
[36] G. M. Shepherd, ed., *The Synaptic Organization of the Brain* (Oxford University Press, Oxford, 1998).